ADHESION LOSS PREDICTION OF A CLIMBING ROBOT THROUGH MAGNETIC FIELD ANALYSIS BY ARTIFICIAL NEURAL NETWORKS

Rodrigo Valério Espinoza
André Schneider de Oliveira
Lúcia Valéria Ramos de Arruda
Flávio Neves Junior
Federal University of Technology, Parana (UTFPR), Automation and Advanced Control System Laboratory (LASCA)
Av. Sete de Setembro, 3165, Rebouças, CEP 80230-901, Curitiba, PR, Brazil
rodrigovespinoza@gmail.com   andreoliveira@utfpr.edu.br   lvrarruda@utfpr.edu.br   neves@utfpr.edu.br

Abstract. *This paper discusses an improvement for an autonomous robot's magnetic climbing system necessary to perform the inspection of metal plates and weld beads in internal/external LPG storage sphere's surfaces. This task typically covers up to 360° in the roll-pitch-yaw angles navigation with respect to the Earth's surface plan. Also, the storage spheres' metal surfaces present non-modeled disturbances (such as surface irregularities, rust dust, welding seams...) that can change the adhesion force, requiring an active control to maintain the force balance needed for trajectory tracking. Classic approaches utilize distance sensors to detect gaps between the wheel and the surface, providing a low-level feedback to the control system that, generally, does not have an active compensation of adhesion, thus, disturbing the robot navigation. Unfortunately this method is inappropriate due to the adhesion system's nonlinear behavior (adhesion force between wheel and surface decreases radically with gaps) and tracking limitations. In order to surmount these problems, an adhesion disturbances recognition system based in artificial neural networks is developed to predict adherence anomalies through magnetic field analysis. This prediction of adherence loss allows the implementation of a new approach to adhesion feedback in robot navigation controllers, that could be used to overcome adhesion disturbances. The proposed system fulfills the inspection tasks by preventing the detachment of one or more wheels and, possibly, the robot's fall without making path deviations.*

Keywords: *Autonomous Robot, Magnetic Adhesion, Magnetic Field Analysis, Neural Network, Disturbance Recognition System*

1. INTRODUCTION

Industry growth and technology improvement demand an increase of robot-based solutions for a great variety of processes. Several of the researches realized to supplement this increasing necessity are related with climbing robots (CR), a multi-task mobile robot system topology applicable to complex environments. These robots can be used in several fields such as industry petrochemical, nuclear and other power plants, which commonly presents hazardous tasks.

The CRs can be applied to different purposes, resulting in a wide mechanical topology diversity (e.g. Chu *et al.* (2010) and Caprari *et al.* (2012)) of which locomotion and adhesion systems are of greatest interest, given that they represent the main interface with the robot's work environment. These systems are very closely attached, hence locomotion and adhesion approaches are not chosen independently. These systems' interaction results some specific characteristics which can be crucial in some tasks performance, and also for the project scope fulfillment.

Common locomotion strategies for climbing tasks are based in legs (e.g., Kim *et al.* (2007)), tracks (e.g., Ben-Tzvi *et al.* (2009)), body translation (e.g., Osswald and Iida (2011)) and wheels (e.g., Schmidt *et al.* (2011)). The adhesion's approaches are diverse (e.g, Silva *et al.* (2008) and Caprari *et al.* (2012)) but the main strategies are based in: suction (e.g., Jiang *et al.* (2009)), gripping (e.g., Guan *et al.* (2011)), adhesives (e.g., Kim *et al.* (2007)) and magnetic force (e.g., Xu and Ma (2002)). A classic approach for robot climbing in metallic surfaces tasks combines magnetic adhesion with wheel locomotion, e.g., works of Fischer *et al.* (2011) and Wu *et al.* (2011).

The inherent characteristic of the magnetic components, typically permanent magnets, guarantees full time adherence without a power source or other auxiliary device which is very convenient since the CR's weight is a crucial point in the project. Although this kind of robot is limited to work exclusively on magnetic surfaces, it can be applied to a broad range of tasks, such as inspection and maintenance tasks in power plants, liquefied petroleum gas (LPG) storage spheres and oil tanks, pipelines and ship hulls.

In scientific community, a great diversity of mechanical solutions for climbing robots is discussed, but the applications are focused on magnetic passive adhesion systems with open loop strategies (e.g. in Fernández *et al.* (2010) and Kalra *et al.* (2006)) which are susceptible to error due to disturbances and can "overthrow" the robot.

The metal surfaces commonly present unmodelled disturbances (such as surface irregularities, rust dust, welding seams, ...) that can change the adhesion force and it requires an active control to maintain the force balance needed for trajectory tracking. An alternative approach to overcome this problem is based on discrete control of the adhesion force through distance variation between permanent magnets and surface, as seen in Wu *et al.* (2011) and Oliveira *et al.* (2010). However, this kind of approach is unable to make fast and precise adjustment of the adhesion (what is often required) due to the nonlinear behavior of the magnets, i.e., a little increase in the gap between magnet and surface strongly decreases the adhesion force. Additionally, gap between wheel and surface is not the only way to reduce the magnetic adhesion force, other factors such as surface's material magnetic characteristics and surface thickness also reduces the magnetic adhesion force.

This paper presents the active adhesion force control with detachment prediction for CR autonomous navigation in a LPG storage sphere. This work is organized in the following manner. Section (2) shows the robot's concept. Section (3) describes the robot's control architecture and Sections (4) and (5) present respectively experimental results and conclusion.

2. ROBOT CONCEPT

2.1 The Inspection Environment and Design Requisites

Storage spheres, as presented in Fig. (1), are metal structures commonly used in the petrochemical sector to store liquefied gases in high pressures. Their advantage is the reduced dimension compared to cylindrical tanks with the same load capacity, hence cheaper.

Figure 1. LPG storage sphere.

The inspection of LPG tanks is a hazardous and complex process due to the insalubrious environment (especially inside the tank), size of the inspection area and mainly to the height (about 18 m) of the spheres therefore, the process automation is highly recommended.

Autonomous robotic inspection consists in an autonomous navigation task in which a robot covers the entire surface of the object being inspected and allows the detection of environment's inconsistencies. In this case, the climbing robot must navigate in planes including the perpendicular to the Earth's surface thus, the gravitational disturbance is highly important and cannot be neglected.

According to Chu *et al.* (2010), a climbing robot project must take into account the following aspects:

- *Weight*: moving against gravity has direct influence of weight force and also the heavier the robot, the bigger is its energy consumption;

- *Mobility*: in some situations, the robot must be able to move in complicated paths in order to perform certain tasks;

- *Adherence*: the climbing ability is directly related with the adherence system and its flexibility to deal with external factors, such as gravity.

2.2 Robot Design

The robot's mechanical structure is showed in Fig. (2), it consists of two parallel sets of fixed wheels (not steerable). Each set is linked by a Vee belt, hence two motors control the movement of four wheels; the robot has two degrees of freedom. The wheel sets are misaligned so that, when passing small obstacles (e.g., weld seams), two parallel wheels do not decrease their adhesion forces at the same time.
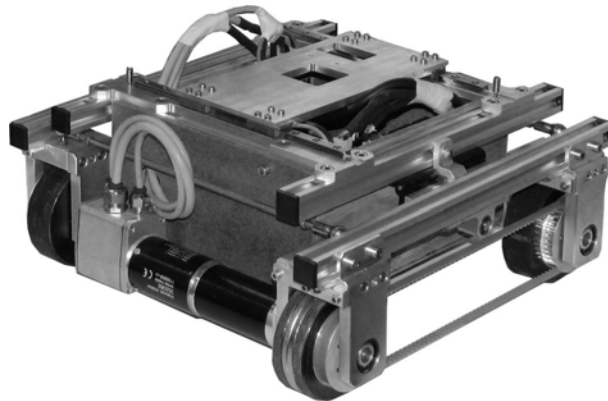

Figure 2. Robot's mechanical structure.

The wheels were designed so the robot could support its own weight, the inspection equipment and the umbilical cord. Each wheel consists in a set of two ring shaped neodymium magnets positioned between two steel disks and attached by screws with low magnetic permeability, the set is covered by a high hardness polyurethane rubber. The Fig. (3) shows one of the wheels with the transmission pulley attached, its magnetic force is approximately 440N. More details about the robot's mechanical construction can be found in Rovani (2013) and de Oliveira *et al.* (2012).
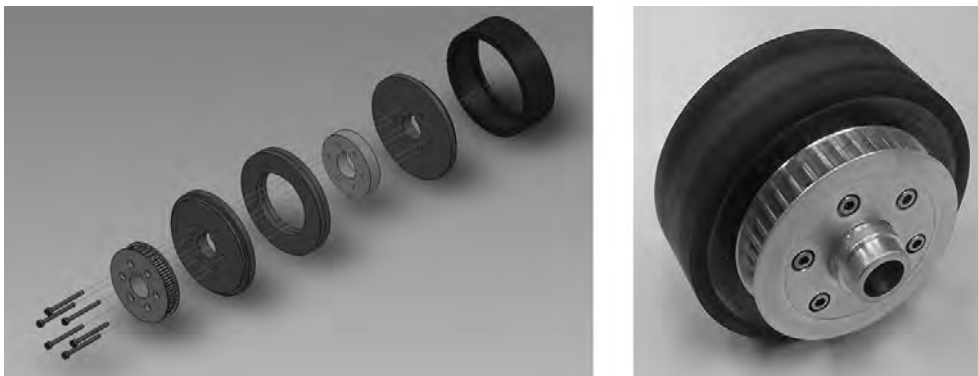

Figure 3. Magnetic wheel's exploded vision (left) and built magnetic wheel (right).

Figure (4) shows the robot's devices diagram. The scheme shows that the robot does not have the inspection module. The ultrasonic inspection is an independent module that is only carried by the robot. The main requisite of the robot is to perform a smooth navigation that fulfills the navigation requirements allowing a stable inspection.
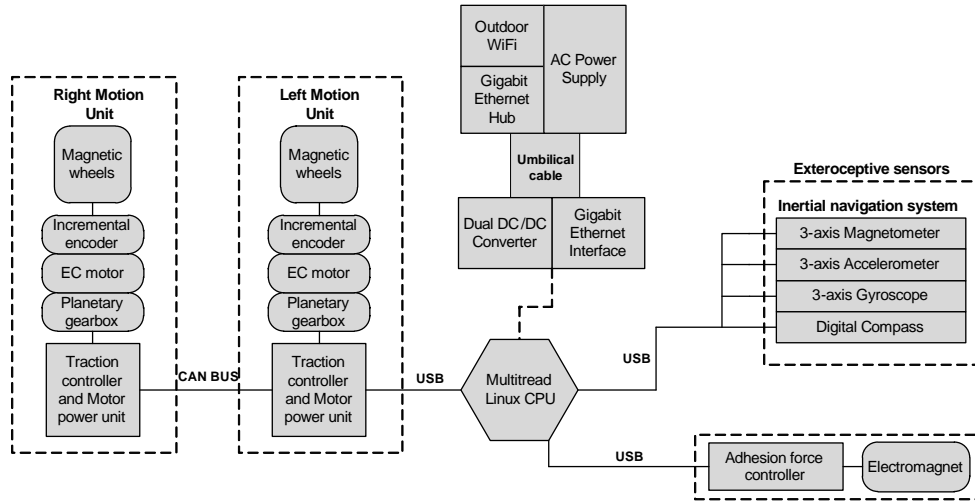
Figure 4. Robot's device diagram.

2.3 Kinematic Model

The robot's kinematics analysis is made assuming that the robot is situated on a global reference plane represented by the system (X_G, Y_G, Z_G) as exhibited in Fig. (5).
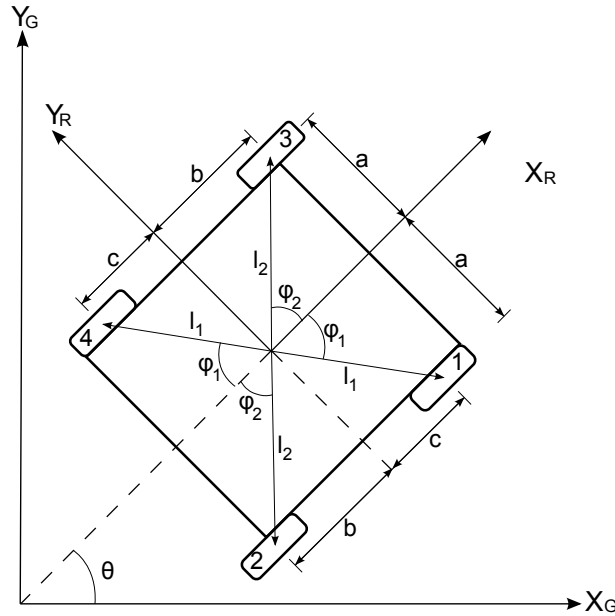

Figure 5. Parameters utilized in the robot's kinematic model.

The robot's reference system is represented by (X_R, Y_R, Z_R), positioned in the chassis center and rotated by de θ in respect of the global system. The robot's pose is represented in respect to the global system as,

$$\xi_G = [\ x \quad y \quad \theta\ ]^T. \tag{1}$$

The robot in both systems, ξ_G and ξ_R, has same angular velocity $(\dot{\theta}_G = \dot{\theta}_R)$ and $(\dot{x}, \dot{y})$ linear velocities related by,

$$\dot{\xi}_R = R(\theta)\dot{\xi}_G, \tag{2}$$

where R is the rotational matrix,

$$R(\theta) = \begin{bmatrix} cos(\theta) & sin(\theta) & 0 \\ -sin(\theta) & cos(\theta) & 0 \\ 0 & 0 & 1 \end{bmatrix}. \tag{3}$$

The robot's kinematic model can be obtained by the union of kinematic constraints (rolling and sliding) of its wheels. To develop the model, its necessary to describe the wheels with respect to the robot's system. Table (1)

gathers the three parameters that describe the wheels. The parameters are expressed in polar coordinates such that l is the distance of the wheels center to the system's origin $O(X_R, Y_R, Z_R)$, α is the rotation angle in Z_R and β is the angle between the wheel plane and the robot's chassis.

Wheel	l	α	β
1	l_1	$-\varphi_1$	$\pi/2 + \varphi_1$
2	l_2	$-\pi + \varphi_2$	$3\pi/2 - \varphi_2$
3	l_2	φ_2	$\pi/2 - \varphi_2$
4	l_1	$\pi - \varphi_1$	$-\pi/2 + \varphi_1$

Table 1. Wheels' parameters.

The rolling constraint ensure that all wheel rotation results is converted in robot's displacement (there is no skid), hence,

$$[D_a \ D_b \ D_c]R(\theta)\dot{\xi}_G - r\dot{\varphi} = 0, \tag{4}$$

where,

$$\begin{bmatrix} D_a \\ D_b \\ D_c \end{bmatrix} = \begin{bmatrix} sen(\alpha + \beta) \\ -cos(\alpha + \beta) \\ -lcos(\beta) \end{bmatrix}. \tag{5}$$

The second constraint imposed is the lateral sliding one, that establishes that the wheel cannot displace in the plane orthogonal to its,

$$[C_a \ C_b \ C_c]R(\theta)\dot{\xi}_G = 0, \tag{6}$$

where,

$$\begin{bmatrix} C_a \\ C_b \\ C_c \end{bmatrix} = \begin{bmatrix} cos(\alpha + \beta) \\ sen(\alpha + \beta) \\ lsen(\beta) \end{bmatrix}. \tag{7}$$

The union of the rolling and sliding constraints (Eqs. (4) and (6)), for every wheel, results the kinematic arrangement,

$$\begin{bmatrix} D \\ C \end{bmatrix} R(\theta)\dot{\xi}_G = \begin{bmatrix} J_R\dot{\varphi} \\ Z \end{bmatrix}, \tag{8}$$

where D and C are 4×3 matrices containing the rolling and sliding constraints coefficients , J_R is a 4×4 matrix which diagonal relates the wheel's radius, $\dot{\varphi}$ is a 4×1 matrix with the wheel's angular velocities $[\dot{\varphi}_1 \ \dot{\varphi}_1 \ \dot{\varphi}_2 \ \dot{\varphi}_2]^T$ and Z is a 4×1 matrix of zeros.

The robot's inverse differential kinematics is defined as,

$$\dot{\varphi} = J^{-1}\dot{\xi}_G, \tag{9}$$

where,

$$J^{-1} = \begin{bmatrix} J_R^{-1}D \\ C \end{bmatrix} R(\theta). \tag{10}$$

From the Eq. (9) the robot's direct differential kinematics equation is defined,

$$\dot{\xi}_G = J\dot{\varphi}. \tag{11}$$

The kinematic model validation is accomplished by a curved trajectory application. The actuator responsible to move wheels 1 and 2 performs a trapezoidal velocity profile, while the actuator that commands the remaining wheels performs a triangular velocity profile. Figures (6) and (7) shows, respectively, the actuators' velocity profiles and the robot's performed trajectory with origin in (0,0).
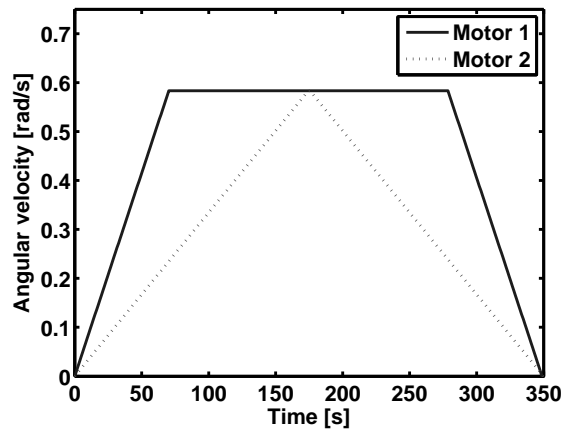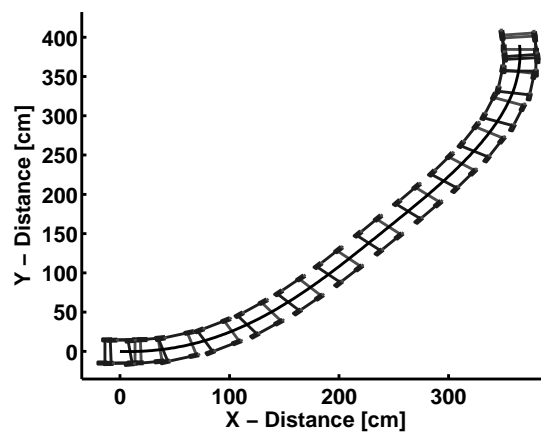
Figure 6. Motors' velocity profile.

Figure 7. Simulated trajectory.

3. CONTROL ARCHITECTURE

The functional behavior of the robot controller is divided in two modes: autonomous and non-autonomous. In non-autonomous mode, the robot is fully controlled by a operator. In autonomous mode, the trajectory planning and system tuning are the initial procedures that are processed in a sequential manner. The operational stages (i.e., navigation and inspection) are executed of parallel manner with processing distributed in dedicated processors. Figure 8 shows the internal behavior of the robot controller.

The climbing strategy is compound by passive and active response, the robot's wheels act with constant magnetic characteristics while the electromagnet gives a continuous control over the applied magnetic force. The magnetic force must be controlled when the robot finds and obstacle, such as a welding seam, that makes one of the wheels to loose part of its adherence while overpassing it. Figure (9) shows the adhesion control system, which is detailed in Sections (3.1) and (3.2).
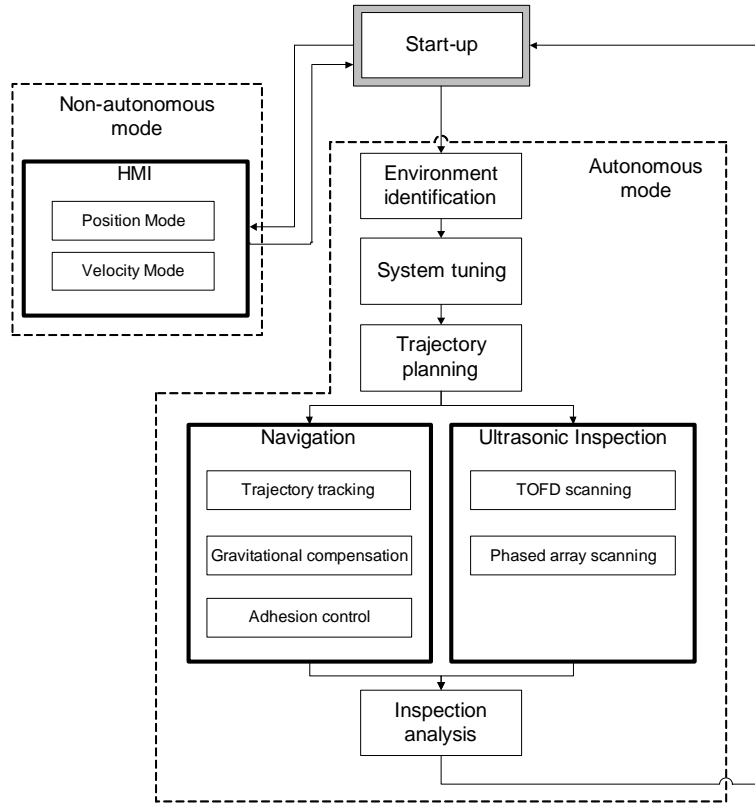
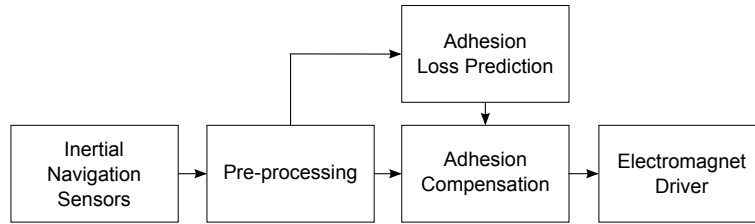Figure 8. Internal behavior of the robot controller.

Figure 9. Adhesion control scheme.

3.1 Adhesion Control

The superficial adherence when navigating inside a gas storage sphere depends directly of the gravitational influence on the normal force (F_N) caused by the contact surface. However, mobile robots usually have degrees of freedom parallel to the contact surface and the normal force can restrict the adhesion. To avoid this effects, magnets are often used always in contact with the surface in order to cancel gravitational force ($G_{Z'}$). But disturbances during navigation may temporarily or permanently reduce magnetic adherence, e.g., one of the goals of gas storage spheres inspection is the welding seam inspection and when passing over these lines the superficial adherence is modified. Passive adhesion, i.e., through permanent magnets, do not allow active control of superficial adhesion and can make the robot fall when a disturbance is occurring. One way of preventing such disturbances is the inclusion of an adhesion force active control strategy by the use of passive permanent magnets (F_P) for usual support and an electromagnet (F_A) for the active control of adhesion disturbances, as shown in Fig.(10)

The superficial adherence is designed through Newton's laws of motion, and its limit is the balance of forces perpendicular to the surface's plan acting on rigid body ($\sum F_z = 0$). However, in balance, any disturbance force would drop the robot. In order to avoid these effects, a minimum adhesion limit for the system is established, i.e., the reference of the controller will be the minimum adhesion limit ($\sum F_z = F_{desired}$). The equation of forces for superficial adhesion on the inside of a gas storage sphere is described as

$$F_{Adh(t+1)} = F_{N(t)}cos(\phi_{(t)}) - F_{P(t)} - F_{A(t)} + F_{dist(t)}, \tag{12}$$

where, F_N is the measured normal force, F_P is the passive force of permanent magnets, F_A is the active force of electromagnet, F_{dist} is the force of disturbance and ϕ is the measured spatial orientation vector.
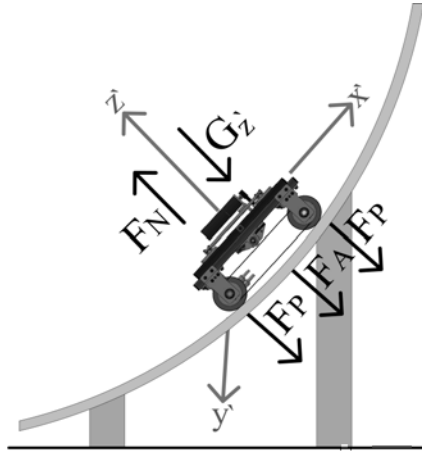
Figure 10. Force balance of active adhesion control.

The electromagnet will be used by the control strategy to maintain the adhesion force greater than the minimum limit (F_{des}), i.e., the active adhesion control is modeled as

$$F_{A(t+1)} = F_{N(t)}cos(\phi_{(t)}) - F_{P(t)} + F_{des(t)} + K_A\tilde{e}_f, \tag{13}$$

where, F_{des} is the limit of the adhesion force, K_A is the adhesion gain and $\tilde{e}_f$ is the adhesion error.

3.2 Adhesion Loss Prediction

The adhesion compensation system, in order to work, must receive as a feedback an adhesion error signal. The adhesion loss prediction system objective is to identify the moments when the electromagnet activation is need therefore, to provide the error signal $\tilde{e}_f$, as expected in Eq. (13).

The difficulty to create a model that solve the prediction problem is significant, because the measured magnetic field may radically change due to numerous factors. Depending on the position of the magnetic field sensor (installed place in the robot's chassis), the action of some wheels may be more (closer to the sensor) or less perceived. Ideally the sensor should be closest as possible and equidistant to the 4 wheels, which is not always possible. Besides the sensor's position, changes in the robot's mechanical/structural topology and introduction of new components may change the profile of the magnetic field measured. These factors encourage the use of artificial neural networks (ANN) to solve the identification problem.

The objective is to construct a ANN capable to identify magnetic field force profiles enabling the correlation between magnetic field force and magnetic adhesion. The target behaviour is showed in Fig. (11).
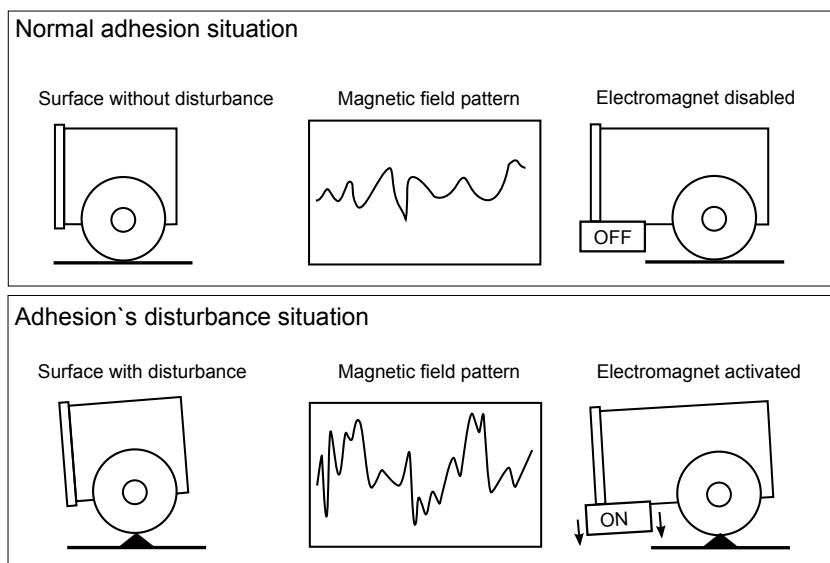

Figure 11. Adhesion control action.

The designed ANN is a multilayer perceptron with one hidden layer. Figure (12) shows the ANN, where

squares represent data and circles represent perceptron neurons. The quantity of neurons and hidden layers were chosen by performance simulations. The network receives 9 inputs (explained in Tab. (2)), which are filtered data from the inertial navigation sensor. The output indicates adhesion loss and the wheel in which it is occurring.
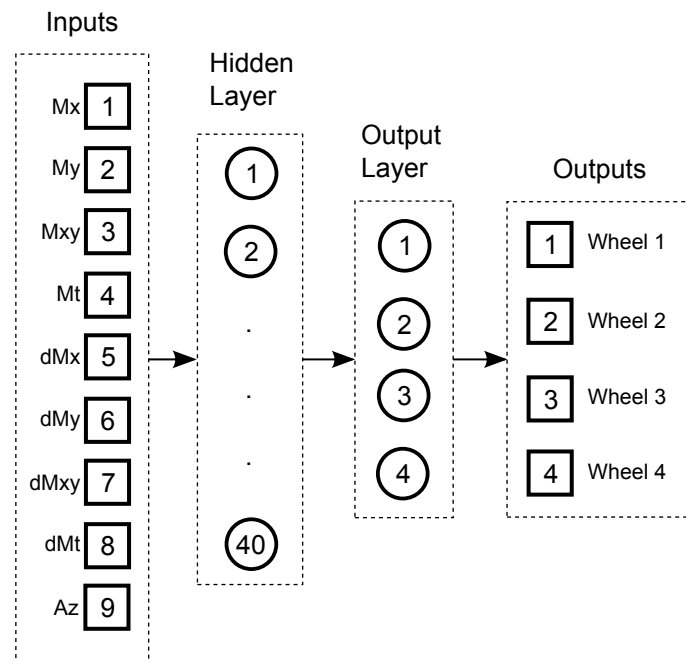

Figure 12. Designed ANN.

Abbreviation	Meaning
M_X	Magnetic field force on the X axis
M_Y	Magnetic field force on the Y axis
M_{XY}	Resultant magnetic field force of the X and Y axis
M_T	Total resultant magnetic field force
dM_X	Derivative of M_X
dM_Y	Derivative of M_Y
dM_{XY}	Derivative of M_{XY}
dM_T	Derivative of M_T
A_Z	Acceleration on the Z axis

Table 2. ANN inputs.

The ANN was trained using the Resilient Backpropagation method, which was the most efficient (fast training and lowest error achievement). The training set was composed by 192105 data acquired from several detachment tests. The error obtained in the best epoch (200) of the training process was 0,63%.

4. EXPERIMENTAL RESULTS

The designed ANN was evaluated using the data of 3 new detachment tests. The first 2 tests involved independent detachment, i.e. just one wheel perturbed at a time. In the last test more than one will adherence were reduced at a time. Figures (13) and (14) show, respectively, the ANN experiment for the right (wheels 1 and 2) and left wheels set (wheels 3 and 4).
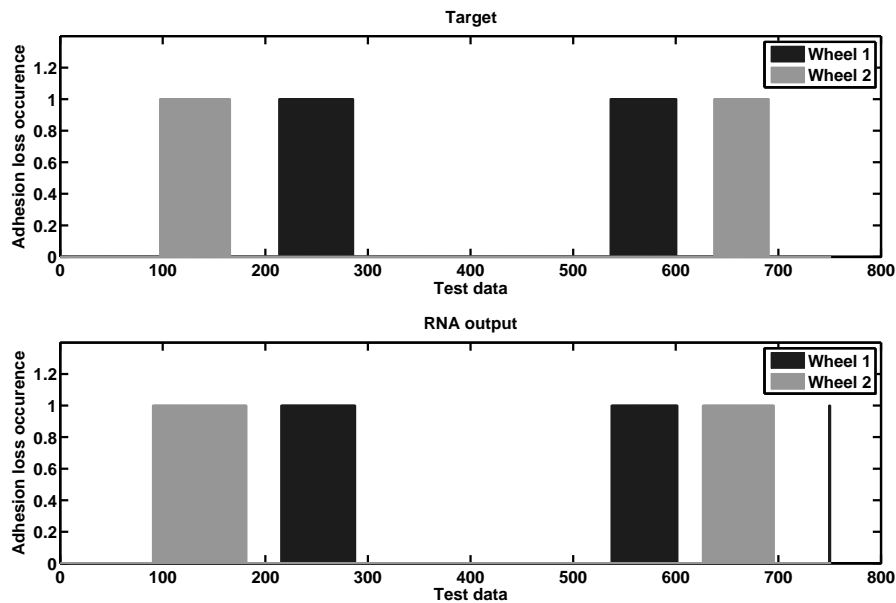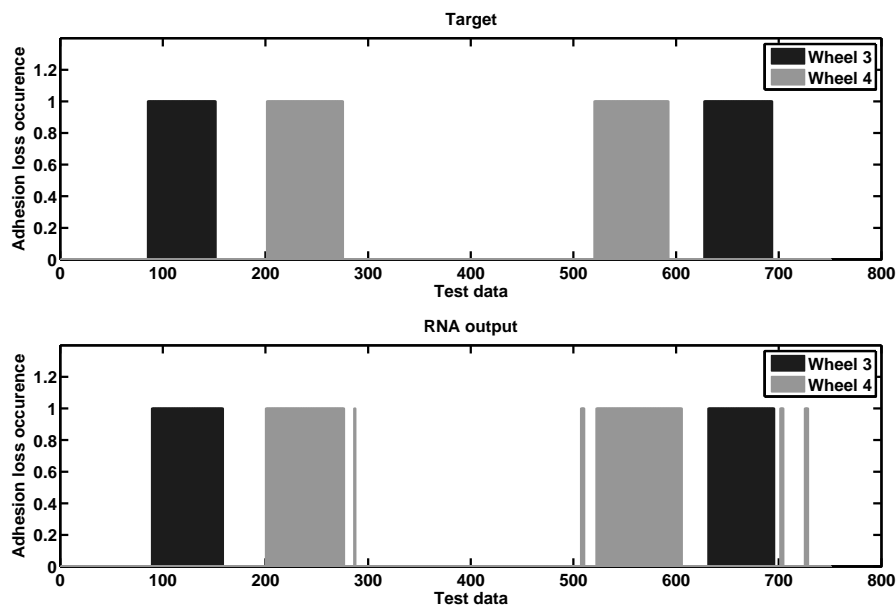
Figure 13. ANN test for wheels 1 and 2.

Figure 14. ANN test for wheels 3 and 4.

The ANN's efficiency is measured by the similarity between the target and ANN's output. It can be seen that the ANN's outputs profile are very close to the target. Table (3) shows the efficiency of the network.

Performance [%]	Independent disturbances	Simultaneous disturbances
Wheel 1	97,79	96,14
Wheel 2	100	72,39
Wheel 3	92,80	77,25
Wheel 4	93,93	48,83
Overall	98,25	84,34

Table 3. Adhesion loss identification outcome.

5. CONCLUSION

This paper presented a climbing robot intended to be used in inspection of liquefied petroleum gas storage spheres. The system is stabilized by an active adhesion controller which uses a electromagnet as additional support to the passive permanent magnets of the wheels. An artificial neural network is employed to predict adhesion losses by magnetic field analysis, providing a feedback signal to control strategy.

The ANN, applied to adhesion loss prediction, resulted a reliable system capable to fulfill the adhesion control system requisites. Although the system response is binary identifying the detachment occurrence (1 - adhesion loss, 0 - adhesion normal), the experiments results showed that the strategy is robust and ,therefore, is capable for improvement. The ANN's system next step will be the prediction of detachment as well as identification of the adhesion reduction's intensity.

Future works will focus in the architecture's control, intelligent autonomous navigation, sensor fusion and navigation/mapping system, surface inspection techniques and identification of other parameters by magnetic field analysis.

6. ACKNOWLEDGEMENTS

7. REFERENCES

Ben-Tzvi, P., Ito, S. and Goldenberg, A., 2009. "A mobile robot with autonomous climbing and descending of stairs". *Robotica, Cambridge Univ Press*, Vol. 27, pp. 171–188.

Caprari, G., Breitenmoser, A., Fischer, W., Hürzeler, C., Tâche, F., Siegwart, R., Nguyen, O., Moser, R., Schoeneich, P. and Mondada, F., 2012. "Highly compact robots for inspection of power plants". *Journal of Field Robotics*, Vol. 29, pp. 47–68.

Chu, B., Jung, K., Han, C. and Hong, D., 2010. "A survey of climbing robots: Locomotion and adhesion". *International Journal of Precision Engineering and Manufacturing*, Vol. 11, pp. 633–647.

de Oliveira, A.S., de Arruda, L.V.R., Junior, F.N., Espinoza, R.V. and ao Pedro Battistella Nadas, J., 2012. "Adhesion force control and active gravitational compensation for autonomous inspection in lpg storage spheres." In *Robotics Symposium and Latin American Robotics Symposium (SBR-LARS)*. pp. 232–238.

Fernández, R., González, E., Feliú, V. and Rodríguez, A., 2010. "A wall climbing robot for tank inspection. an autonomous prototype". *Conference on IEEE Industrial Electronics Society (IECON)*, pp. 1424–1429.

Fischer, W., Caprari, G., Siegwart, R. and Moser, R., 2011. "Locomotion system for a mobile robot on magnetic wheels with both axial and circumferential mobility and with only an 8-mm height for generator inspection with the rotor still installed". *IEEE Transactions on Industrial Electronics*, Vol. 58, pp. 5296–5303.

Guan, Y., Jiang, L., Zhu, H., Zhou, X., Cai, C., Wu, W., Li, Z., Zhang, H. and Zhang, X., 2011. "Climbot: A modular bio-inspired biped climbing robot". In *Intelligent Robots and Systems (IROS), 2011 IEEE/RSJ International Conference on*. pp. 1473–1478.

Jiang, Z., Li, J., Gao, X., Fan, N. and Wei, B., 2009. "Study on pneumatic wall climbing robot adhesion principle and suction control". In *Robotics and Biomimetics, 2008. ROBIO 2008. IEEE International Conference on*. pp. 1812–1817.

Kalra, L., Gu, J. and Meng, M., 2006. "A wall climbing robot for oil tank inspection". *IEEE International Conference on Robotics and Biomimetics (ROBIO)*, pp. 1523–1528.

Kim, S., Spenko, M., Trujillo, S., Heyneman, B., Mattoli, V. and Cutkosky, M.R., 2007. "Whole body adhesion: hierarchical, directional and distributed control of adhesive forces for a climbing robot". *IEEE International Conference on Robotics and Automation*, pp. 1268 –1273.

Oliveira, A., Silva, M. and Barbosa, R., 2010. "Architecture of an wheeled climbing robot with dynamic adjustment of the adhesion system". *IEEE International Symposium on Intelligent Systems and Informatics*

(SISY), pp. 127–132.

Osswald, M. and Iida, F., 2011. "A climbing robot based on hot melt adhesion". In *Intelligent Robots and Systems (IROS), 2011 IEEE/RSJ International Conference on.* pp. 5107–5112.

Rovani, A., 2013. "Desenvolvimento do protótipo de um robô para inspeção de cordões de solda em superfícies metálicas verticais". *Trabalho de Conclusão de Curso - Engenharia Industrial Mecânica - Universidade Tecnológica Federal do Paraná, Curitiba*, p. 117.

Schmidt, D., Hillenbrand, C. and Berns, K., 2011. "Omnidirectional locomotion and traction control of the wheel-driven, wall-climbing robot, cromsci". *Robotica, Cambridge Univ Press*, Vol. 29, pp. 991–1003.

Silva, M., Machado, J. and Tar, J., 2008. "A survey of technologies for climbing robots adhesion to surfaces". In *Computational Cybernetics, 2008. ICCC 2008. IEEE International Conference on.* pp. 127–132.

Wu, M., Gao, X., Yan, W., Fu, Z., Zhao, Y. and Chen, S., 2011. "New mechanism to pass obstacles for magnetic climbing robots with high payload, using only one motor for force-changing and wheel-lifting". *Industrial Robot: An International Journal*, Vol. 38, pp. 372–380.

Xu, Z. and Ma, P., 2002. "A wall-climbing robot for labelling scale of oil tank's volume". *Robotica, Cambridge Univ Press*, Vol. 20, pp. 209–212.

8. RESPONSIBILITY NOTICE

The authors are the only responsible for the printed material included in this paper.